Supplementary Information for

Multiplex Serum Cytokine Immunoassay Using Nanoplasmonic Biosensor Microarrays

Pengyu Chen[†]*, Mengting-Chuang*[†]*, Walker McHugh*[‡]*, Robert Nidetz*[†]*, Yuwei Li*[†]*,Jianping Fu,*[†,§]*, Timothy T. Cornell*[‡]*, Thomas P. Shanley*[‡]*, and Katsuo Kurabayashi*[†,⊥,*]

[†]Department of Mechanical Engineering, University of Michigan, Ann Arbor, Michigan, 48109, USA.

[‡]Department of Pediatrics and Communicable Diseases, University of Michigan, Ann Arbor, Michigan, 48109, USA.

[§] Department of Biomedical Engineering, University of Michigan, Ann Arbor, Michigan, 48109, USA.

[⊥]Department of Electrical Engineering and Computer Science, University of Michigan, Ann Arbor, Michigan, 48109, USA.

[*]To whom correspondence should be addressed. E–mail: katsuo@umich.edu

1) **Characterization of gold nanorods**:

We purchased the gold nanorods (AuNRs) used in this study (Fig. S1A) from NanoSeedz in aqueous cetrimonium bromide (CTAB, 0.1 M) buffer. These nanorods were originally synthesized using the standard seed-mediated growth method. This yielded single-crystalline nanoparticles with an average length of 80±5 nm and an average width of 40±3 nm. (Fig. S1B) The CTAB coating on the AuNRs resulted in a positively charged surface with a zeta potential of 42±5 mV (Zetasizer Nano ZS90, Malvern). The extinction spectrum of the AuNRs in solution was obtained using a customized spectrophotometer.[1] The resonance peak wavelength of the AuNR lays around 626 nm, in congruence with the simulation results as shown later in Section 7.

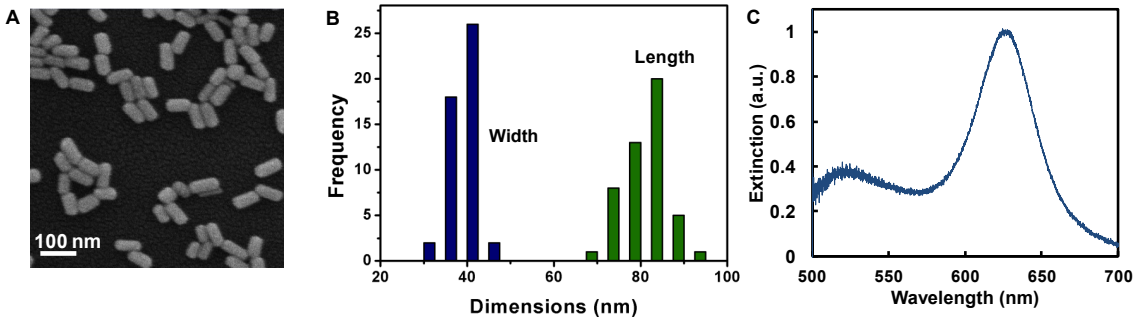

Figure S1. (A) Scanning electron micrograph of AuNRs drop-cast onto a conductive glass substrate. (B) Statistics of the length and width of the AuNRs measured from high magnification electron microscopy in (A). (C) Extinction spectra of AuNRs in solution showing the resonant Rayleigh scattering wavelength at around 626 nm.

2) Gold nanorod microarray fabrication:

Prior to the AuNR microarray fabrication, we constructed a microfluidic flow-patterning mask layer made of PDMS using soft lithography. The mask layer contains multiple sets of parallel microfluidic channels for patterning the AuNR microarrays. Specifically, we

first patterned a mold for the PDMS flow-patterning mask layer within a silicon substrate using deep reactive-ion etching (DRIE) (Deep Silicon Etcher, Surface Technology Systems, Allenton, PA). The mold surface was silanized with (tridecafluoro-1,1,2,2,-tetrahydrooctyl)-1-trichlorosilane vapor (United Chemical Technologies) for 1 hour in vacuum to facilitate subsequent PDMS release. We next poured PDMS prepolymer (Sylgard-184, Dow Corning), prepared by thoroughly mixing a curing agent with a base monomer (wt : wt = 1 : 10), onto the silicon mold and cured it in an oven at 110°C for 4 hrs. The cured PDMS mask layer was then peeled off from the mold to form a microfluidic flow-patterning layer. The layer was cut into multiple pieces, each hole-punched to create inlets and outlets for its channels in further use.

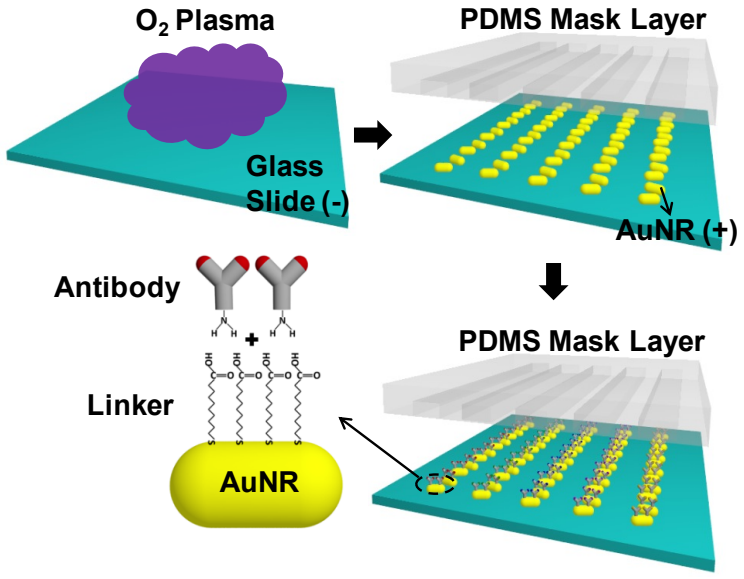

Figure S2. Schematic of the LSPR microarray chip patterning process that entails glass pre-treating, AuNR deposition, and antibody function. The nanorod microarray fabrication was performed using a one-step microfluidic patterning technique assisted by electrostatic attractive interactions between the nanorods and the substrate surface within the microfluidic flow-patterning channels of the PDMS mask layer. Specific antibodies were conjugated to the patterned AuNR microarrays using thiolated crosslinker and EDC/NHC chemistry.

Subsequently, we centrifuged AuNR stock solution (0.2 nM) three times at 5700 rpm for 10 min, and resuspended the pellet in D.I. water to remove excessive CTAB in the solution. The AuNR solution was further diluted 8 times before the microarray fabrication. Glass slides were first treated with Piranha solution (H_2SO_4:H_2O_2 = 3:1 v/v) for 10 min, rinsed thoroughly with D.I. water, and kept in an ultrasonic bath with ethanol for 30 min. We then treated the surfaces of the glass substrates under O_2 plasma for 2 min at 18 W (COVANCE 1-MP, Femto). This created a negatively charged glass surface owing to the dissociated hydroxyl groups existing on the glass, which enabled the glass substrate to attract the positively charged, CTAB stabilized AuNRs onto its surface. Immediately after the surface treatment, one of the microfluidic flow-patterning PDMS mask layer pieces prepared above was non-permanently bonded onto each glass substrate. We then loaded 2 μL of AuNR solution into each channel at a flow rate of 1 μL/min and incubated overnight. The inlets and outlets were sealed with a cover glass to prevent evaporation and avoid dry-out of the AuNR solution during incubation.

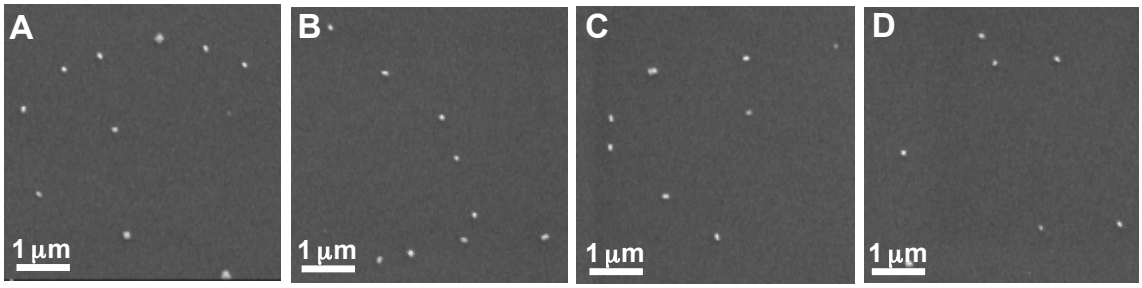

Figure S3. Scanning electron microscope images of AuNR particles within a microarray pattern on a glass substrate. The resulting surface density of the particles is ~ 1 particle per 2.56 μm^2.

After the incubation, we washed all the channels with 100% ethanol to remove unbound AuNRs. This resulted in formation of AuNR microarray patterns on the regions

of the glass surface covered by the channels. The SEM images in Fig. S3 show that the resulting surface density of AuNRs on each microarray is around 1 particle per 2.56 μm^2.

3) Gold nanorod microarray functionalization:

After constructing the AuNR microarray patterns on the glass substrate, we functionalized them within the microfluidic flow-patterning channels constructed above by forming a self-assembled monolayer (SAM) through simple ligand exchange.[2] A stock solution of thiolated alkane 10-Carboxy-1-decanethiol (HS-$(CH_2)_{10}$-COOH) was diluted to 1 mM in 100% ethanol and flown through the patterning channel on the glass substrate. The stronger affinity of the thiol anchor group with the gold surface enabled the thiolated alkane to replace the CTAB coating and serve as a linker to probe antibodies. Here, the thiol anchor group would preferably replace the exposed CTAB groups remaining on the gold surface instead of the CTAB groups buried underneath. Thus, the ligand exchange does not affect the AuNRs' stability on the glass substrate. The antibody linking was performed by way of the antibody binding to the –COOH functional group through standard 1-ethyl-3-[3-dimethylaminopropyl]carbodiimide/N-hydroxysuccinimide (EDC/NHS) coupling chemistry.[3] Briefly, we injected a mixture of 0.4 M EDC (Thermo Scientific) and 0.1 M NHS (Thermo Scientific) at a 1:1 volume ratio in 0.1 M EDC(1-ethyl-3-[3-dimethylaminopropyl]carbodiimide hydrochloride, Thermo Scientific) solution through the microfluidic flow-patterning channels and activated the AuNRs microarray surfaces on the glass substrate. After the surface activation, we diluted primary cytokine antibodies (eBioscience) from 100 to 10 μg/mL in 1x PBS, loaded them into individual channels and incubated them at room temperature for 60 min. This resulted in the construction of six meandering parallel AuNR stripe patterns of 25 μm in

width and 2 cm in length at a pitch of 50 μm on the glass substrate, each functionalized with distinct antibody molecules. These patters formed the LSPR biosensor microarrays affording multiplex detection of six different cytokines. To suppress the non-specific binding on the detection surface, we flew 10μL of 1% BSA (Albumin, from bovine serum, SIGMA) in 1x PBS and 1x casein (5x Casein block solution, Surmodics BioFX) blocking buffer into the microfluidic flow-patterning channels and incubated it for 20 min. During all the process steps, we loaded the reagent solutions using a syringe pump (LEGATO210, Kd Scientific) at 1 μL/min. Between every step, the AuNR microarray surface was thoroughly washed to remove any excessive solutions or molecules using 20 μL of 1x PBS at 3 μL/min.

(4) Optical setup and LSPR microarray imaging measurement:

Following the AuNR microarray antibody functionalization process, we removed the PDMS mask layer from the glass substrate and immediately replaced it with another PDMS layer with sample-flow microfluidic channel arrays. This new PDMS layer was fabricated following the same procedure as described for the construction of the PDMS microfluidic flow-patterning mask layer in supporting information Section 2. During the process of assembling our assay chip, we bonded the new PDMS layer onto the glass substrate such that the sample-flow channel arrays (200 μm (W) x 2.5 cm (L) x 50 μm (H)) were placed perpendicular to the LSPR microarray stripes. We subsequently mounted the constructed microarray assay chip on a motorized X-Y stage (ProScanIII, Prior Scientific, Rockland, MA), manually loaded a sample of ~5 μL into each of the on-chip flow channels using a pipette, and performed automated image scanning at a rate of

180 sensing spots/min. Figure S4 shows the system setup by which we detected and imaged the AuNR microarray arrays based on a dark-field LSPR imaging technique.

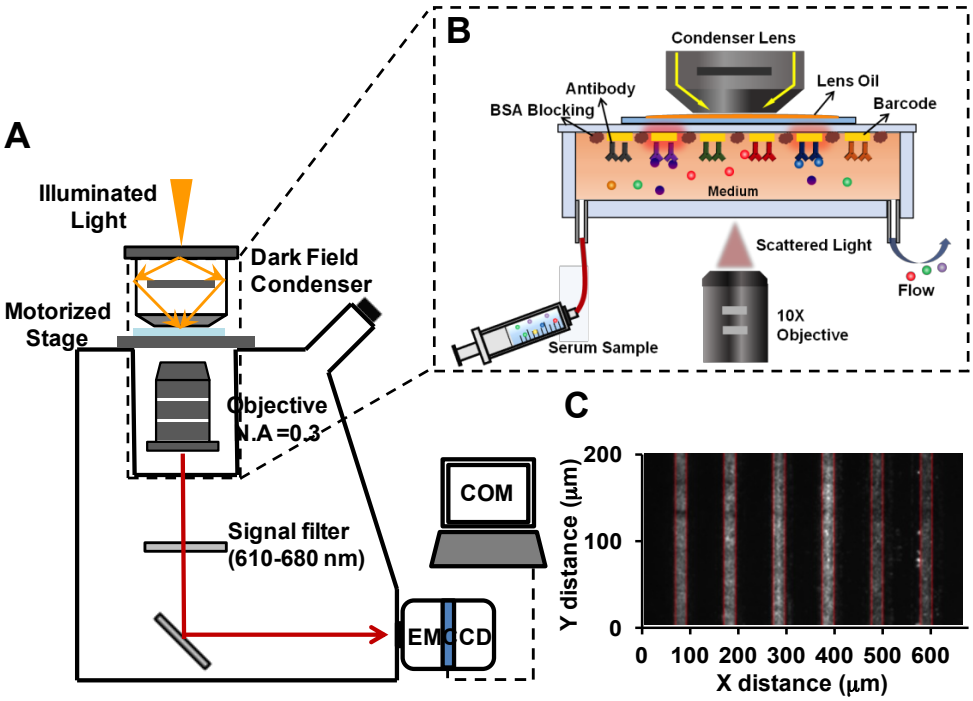

Figure S4. (A) Schematic of the dark-field microscope setup for LSPR microarray immunoassay. (B) Illustration of the LSPR microarray assay protocol using the prepared LSPR microarray chip and dark-field imaging. The chip was mounted on the motorized stage with the back of its glass substrate in contact with the dark-field condenser via lens oil. A sample was injected from the inlet, flown through the sample channel, and collected from the outlet. Different cytokines in the sample were captured by the antibody-conjugated AuNR microarrays. The light scattered from the microarrays was collected by the 10X objective lens beneath the chip and filtered by a band pass filter and imaged by the EMCCD. (C) Microarray images analyzed by customized Matlab program. The program allowed automated microarray image recognition, data acquisition, and signal analysis.

Briefly, the LSPR microarray imaging process started with guiding white illumination light into the dark-field condenser oil lens (n.a. 1.20 to 1.45, Mager Scientific) installed on the inverted fluorescent microscope (Nikon Eclipse Ti-S, Nikon). Binding of analyte molecules onto the nanostructured metal surface of each microarray

induced an increase in the scattering rate of light within a certain spectral band as well as a red shift in the LSPR peak (630 nm for our AuNRs as shown in Figure 1S). We used a band pass filter (610-680 nm) to capture the maximum intensity increase observed for the microarrays during analyte surface binding. We obtained the images of microarrays with the EMCCD camera and recorded them using NIS-Element BR analysis software. A customized Matlab program was used to analyze and quantify the scattering intensity shift for each microarray pattern. The region of interest was automatically selected through an edge detection/background subtraction algorithm, and then the raw data of each pixel was read out and processed.

5) Electromagnetic-field optical simulation on a single gold nanorod upon local refractive index change:

In order to theoretically estimate the limit of detection of the LSPR microarray measurement, we first performed a finite difference time domain (FDTD) simulation and predicted the scattering efficiency on a single AuNR using commercial multi-physics simulation software, COMSOL. Our simulation used the dimensions of the AuNR that were determined by the results of our material characterization in Section 1 of Supplemental Information (40nm in diameter, aspect ratio: 2). The plasmonically decoupled AuNR arrangement in the fabricated microarray patterns (Figure 1 in the main text) allowed us to focus our attention to the LSPR behavior of the single AuNR, which significantly simplified our simulation. The frequency-dependent complex permittivity of gold was derived from the Lorentz-Drude model.[4]

The far-field domain was defined as a spherical shell surrounding the AuNR with a radius identical with half the wavelength of incident light. As the boundary condition of

the simulation, we set a perfectly matched layer of thickness identical to half the incident light wavelength on top of the surface of the far-field domain spherical shell, where the intensity of scattering light from the AuNR exponentially decays. We set the wave vector and electric field polarization of the incident light to be perpendicular and parallel to the orientation of the AuNR, respectively. This excited the longitudinal resonant mode of the AuNR in the simulation. The mesh size was set to be 1 nm on the AuNR surface and no larger than 1/10 of the studied wavelength elsewhere (Fig. S5A). We then calculated the spatial distribution of the electromagnetic field on the far-field plane at varying frequencies with and without the presence of the AuNR to determine the intensity of scattering wave from the AuNR, I_{AuNR}, and the background signal intensity, $I_{backgound}$. The scattering cross section C_{scs} of the AuNR can be determined by integrating the intensity of scattering wave over the surface of the far-field plane Ω as

$$C_{SCS} = \int \frac{I_{AuNR}}{I_{background}} d\Omega \quad (1)$$

and will later be used for our calculation of the limit of detection.

It is worth noting that our simulations only considered the longitudinal resonant mode along the longer axis of the AuNR. In fact, the excited electromagnetic response from a randomly orientated AuNR generally consists of a net contribution from both the longitudinal and transverse modes on the AuNR. However, the transvers mode peak of our AuNR at 522 nm is much weaker than its longitudinal mode peak at 626 nm according to the extinct spectral measurement in Fig. S1C. Furthermore, the full width of half maximum (FWHM) of the longitudinal mode is as narrow as 53 nm. (These values are consistent with our simulation predicting a resonance peak at 625 nm with a FWHM

of 52 nm.) Thus, the contribution of the transverse mode to potential spectrum broadening and shift is negligible, justifying the following simulations not including the transvers mode.

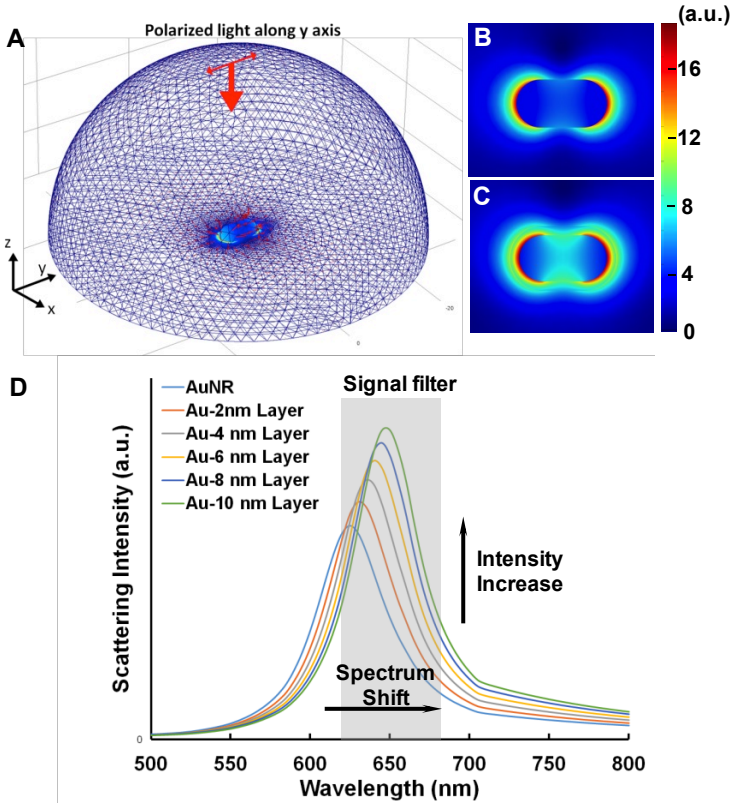

Figure S5. A) FDTD simulation scheme on light scattering response from one single AuNR. B) Near-field LSPR intensity profile of a bare single AuNR excited by incident light. The red (blue) color represents high (low) intensity of the simulated electric field near the AuNR. C) Near-field LSPR intensity enhancement of a single AuNR after coating with a 10 nm thick dielectric material mimicking analyte binding onto an antibody-functionalized AuNR. D) Predicted scattering spectrum (or LSPR spectrum) variation with the thickness of the protein coating on the AuNR.

Next, a simulation was performed to predict how protein binding would enhance LSPR by mapping the spatial distribution of the normalized local electric field intensity ($|E_y|^2/|E_0|^2$) near the surface of a bare AuNR (Fig. S5B and S5C), where $|E_y|^2$ is the intensity of the y-component of the local field and $|E_0|^2$ is the field intensity of the incident light. We also simulated the spectral shift of light scattered from the AuNR due

to protein binding. Our simulation modeled protein binding as formation of a uniform dielectric layer on an antibody-functionalized AuNR surface, which was assumed to cause the near-surface refractive index value to change from 1.33 (water) to 1.5 (hydrated protein).[5] The protein attached to the AuNR surface can be either the analyte or the probe antibody used in our study. The simulation was performed with the thickness of the protein layer ranging from 0 to 10nm with a 2nm increment. Comparing Fig. S5B and Fig. 5C, we learn that coating the AuNR with a 10nm-thick protein layer is predicted to yield a notable enhancement of $|E_y|^2/|E_0|^2$. Figure S5D shows a set of the scattering light spectra of the AuNR coated with the protein layer of varying thickness.

6) Theoretical prediction of the detection limit of the LSPR microarray measurement:

The simulation in Section 5 of Supplemental Information predicts a noticeable spectral red-shift as well as an intensity enhancement for scattering light from the AuNR at a larger protein coating thickness (Fig. S5D). Here, the scattering light intensity is the LSPR signal that we directly observe in our measurements. Using the simulation approach above, we further calculated the quantitative values of the spectral shift and intensity variation of the LSPR signal induced by analyte binding on a single AuNR. The antibody conjugation of the AuNR in our assay was assumed to form a uniform layer of closely packed antibody molecules with a thickness of 7 nm and a refractive index of 1.5.[6] Furthermore, we assumed a theoretical volume called the "sensing volume" on top of the antibody layer (inset of Fig. S6). The thickness of the sensing volume is equivalent to the effective diameter of the analyte molecule (typically 3.4 nm for cytokines).[6] In our model, the refractive index of the sensing volume layer was also set to be 1.5 when the

volume was fully occupied by the analyte molecules. The LSPR signal variation ΔI due to surface binding of a single analyte molecule is then given by:

$$\Delta \mathrm{I} = \frac{\Delta S}{V_s} * \Delta RI * V_a \,, \tag{2}$$

where ΔRI is the refractive index change in the volume of the sensing volume V_s, which was described above, V_a is the volume of the single analyte molecule, and ΔS is the experimentally observed signal difference between before and after loading the analyte molecules onto the AuNR surface. More specifically, ΔS is the analyte adsorption-induced LSPR peak wavelength shift, given by $\Delta S = \frac{\Delta \lambda_p}{RIU}$ for spectrum-shift measurement, where $\Delta\lambda_p$ is the resonance peak shift, and RIU is the refractive index unit (=1). ΔS is the analyte adsorption-induced LSPR intensity (i.e., scattering intensity) shift, given by $\Delta S = \frac{\int_{610}^{680} \Delta C_{scs} \mathrm{d}\lambda}{\mathrm{RIU}}$ for the intensity-based imaging measurement, where $\int_{610}^{680} \Delta C_{scs} \mathrm{d}\lambda$ is the integration of the change in the scattering cross section ΔC_{scs} after the analyte loading over λ = 610-680 nm, which is the optical filter band used in this study (grey area in Fig. S5D). Here, ΔC_{scs} is derived from Eq. (1) in Section 7 of Supplementary Information.

For a given analyte concentration of [A] in the flow channel, the probability of the analyte binding event on the single AuNR surface, θ, can be estimated using Hill-Langmuir isotherm as:[7]

$$\theta = \frac{[A]^n}{K_d + [A]^n} = \frac{1}{1 + (\frac{K_A}{[A]})^n} \,, \tag{3}$$

where K_d is the binding constant determined at the equilibrium dissociation state between the antibody and its engaging antigen, K_A is the ligand concentration producing half

occupation, and n is the Hill coefficient. Alternatively, θ represents the ratio of the number of occupied binding sites over the total number of sites available for analyte binding.

The total analyte binding sites on a single AuNR particle N_S is given by

$$N_s = \frac{(4*\pi R_{Au}^2+2\pi R_{Au}(L_{Au}-2R_{Au}))}{\pi R_{Anti}^2} \quad (4)$$

where R_{Au} and R_{anti} are the radii of the AuNRs and the antibody, respectively, and L_{Au} is the length of the AuNRs. Assuming the AuNR deposition density per unit area within the detection channel to be D, the overall signal intensity change ΔI_A collected from the microarray sensing area can be calculated by:

$$\Delta I_A = \frac{\Delta I}{D} * D * N_s * \left(\frac{1}{1+(\frac{K_A}{[A]})^n}\right) . \quad (5)$$

The LOD of the analyte for LSPR microarray can then be determined when the signal change equals to the system signal uncertainty, $U = \sqrt{{U_{sys}}^2 + {U_{fit}}^2}$, where U_{syi} is the uncertainty due to the detection system and U_{fit} is the uncertainty due to the peak fitting when gathering the scattering spectrum. Therefore, we can obtain:

$$U = \Delta I * N_s * \left(\frac{1}{1+(\frac{K_A}{[A]})^n}\right). \quad (6)$$

Combining Eq. (2) and (5) allows us to analytically estimate the LOD of LSPR microarray as:

$$\mathrm{LOD[A]} = K_A * \left(\frac{\frac{S(r)}{V_S}*\Delta RI*V_a*N_s}{\sqrt{{U_{sys}}^2+{U_{fit}}^2}} - 1\right)^{-1/n} . \quad (7)$$

To estimate the sensitivity improvement of our LSPR microarray over the conventional spectrum-based LSPR measurement, we quantified the signal-to-noise ratio upon an analyte binding event using first order Langmuir equation in Eq. (7). The total available binding sites on one single AuNR (40 nm (W) × 80 nm (L)) can be calculated to be ~361. In an extreme case where the AuNR surface is fully occupied, the spectrum shift ($\Delta\lambda$) is 5.1nm and the scattering cross section change (ΔC_{scs}) integrated from 610nm to 680nm is 7.2% as shown in Figure S6.

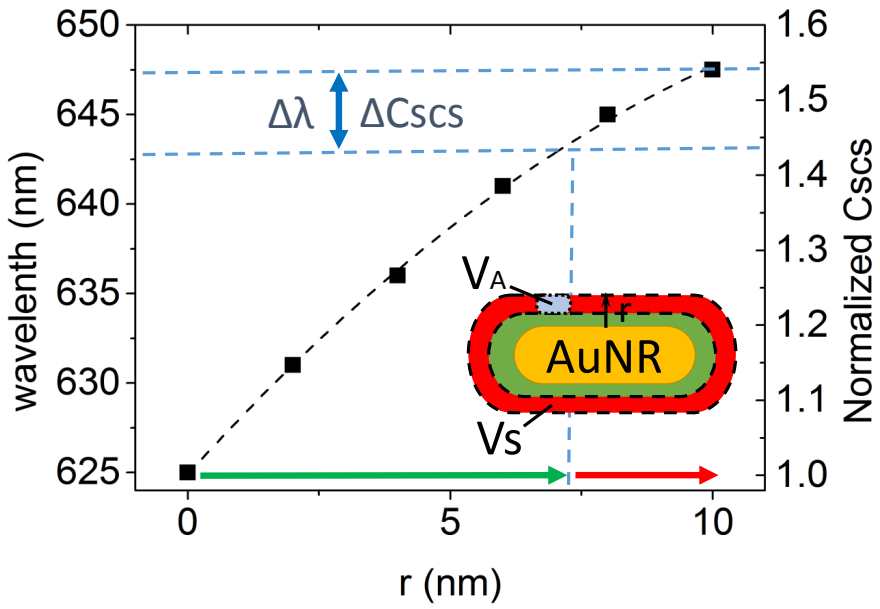

Figure S6. Calculated scattering spectrum peak wavelength (alternatively, scattering cross section normalized by the value for a bare AuNR surface) as a function of the thickness of protein layer covering the AuNR surface, *r*. The inserted figure shows the antibody shell layer (green) at $0 < r < 7$ nm and the analyte shell layer (red) at $7 < r < 10$ nm. From the plot, the spectrum shift ($\Delta\lambda$) and scattering cross section change (ΔCscs) were calculated for the maximum value of *r*, where a 3nm-thick analyte layer is formed on the antibody-coated AuNR.

According to the most recent study using a spectrum-based nanorod LSPR biosensor,[8] the researchers' experimental setup (incandescent white light source, CCD

detection of scattering) yielded a signal variance of $U_{spectrum}$ = 0.3 nm. The uncertainty due to the sensor and signal processing unit in our system $U_{intensity}$ = 0.11% was determined by measuring blank samples. Substituting these numbers into Eq. (7) allows us to calculate the ratio of the LOD of our intensity-based LSPR microarray platform, $LOD_{intensity}$, to that of the conventional spectrum-shift measurement technique, $LOD_{spectrum}$, as:

$$\frac{LOD_{\text{int}ensity}}{LOD_{spectrum}} = [(\frac{\Delta I_{spectrum} * N_s}{U_{spectrum}} - 1) / (\frac{\Delta I_{\text{int}ensity} * N_s}{U_{intensity}} - 1)] = \sim \frac{1}{10} \quad (7)$$

Thus, we estimate that our technique reduces the LOD by a factor of ~10 as compared to the conventional LSPR detection scheme.

7) AuNR microarray intensity and LSPR microarray signal variance

We characterized the structural variance across the AuNR microarrays deposited on a common glass substrate from scanned dark-field images taken for their calibration measurements (Fig. S7A). The upper panel in Fig. S7A shows the line intensity profile of 24 consecutive AuNR microarrays on the same chip. The image data indicate an average intensity of ~ 21,000 with a coefficient of variance (CV) around 8% across all the microarrays. It reveals the consistency of our fabrication technique in producing microarray stripes with good array-to-array structural uniformity. Such uniformity allowed us to obtain a CV of ~7% or lower across calibration data points taken for 10 microarray stripes on the same chip at a given analyte (TNF-α) concentration (Fig. S7B). The result verified the high reproducibility and accuracy of our LSPR microarray measurements using these microarrays.

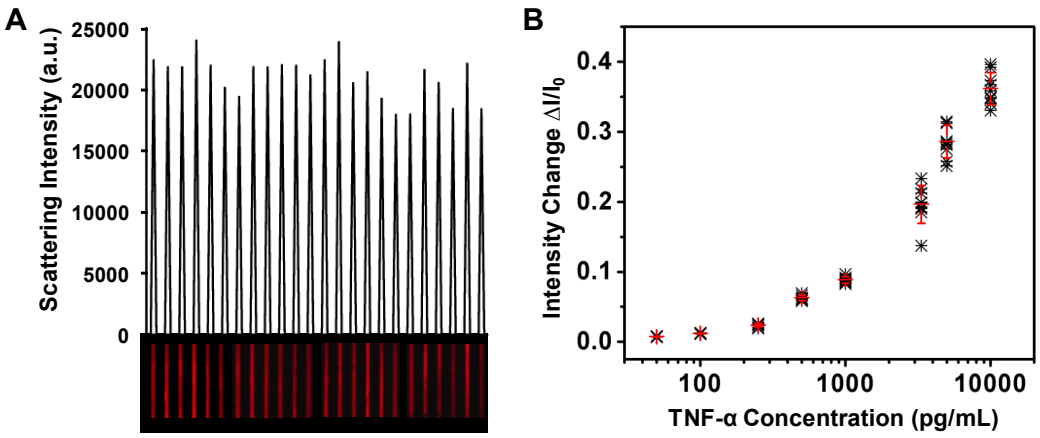

Figure S7. (A) Line intensity profile of the uniformly fabricated AuNR microarrays, which was measured using dark-field imaging microscopy. (B) Calibration plots showing the LSPR microarray signal variation with recombinant TNF-α concentration, where each star represents an individual measurement data point. The average intensity change values and standard derivation are shown in red lines.

8) System uncertainty and limit of detection of LSPR microarray

In order to characterize the uncertainty and limit of detection of our LSPR microarray system, we performed a control experiment measuring the variance of the background signal with antibody-conjugated AuNR microarrays with no cytokines loaded. The average system uncertainty was calculated to be ~0.11%, which was determined by the minimum distinguishable signal equivalent to a confidence factor set to be 3 times the standard deviation of the background noise (σ). The detection limits of the target cytokines were thus obtained from $3\sigma/k_{slope}$, where k_{slope} is the slope of the regression of the calibration curves using sigmoidal curve-fitting.

Cytokine	Blank S.D. (σ) (%)	U_{system} (3σ) (%)	k_{slope} (%)*(pg/mL)$^{-1}$	LOD=3σ/k_{slope} (pg/mL)
IFN-γ	**0.022**	**0.065**	**0.010**	**6.46**
TNF-α	**0.034**	**0.103**	**0.009**	**11.43**
IL-2	**0.069**	**0.206**	**0.010**	**20.56**
IL-4	**0.031**	**0.092**	**0.020**	**4.60**
IL-6	**0.038**	**0.113**	**0.010**	**11.29**
IL-10	**0.030**	**0.088**	**0.008**	**10.97**

Table S1. The LOD's of target cytokines were determined from the minimum distinguishable analytical signal defined by $3\sigma/k_{slope.}$, where σ is the standard derivation of the LSPR microarray signals from blank samples, and k_{slope} is the regression slope obtained from the calibration curves using sigmoidal curve-fitting.

Supplementary Reference

(1) Oh, B. R.; Huang, N. T.; Chen, W.; Seo, J.; Chen, P.; Cornell, T. T.; Shanley, T. P.; Fu, J.; Kurabayashi, K. Integrated Nanoplasmonic Sensing for Cellular Functional Immunoanalysis Using Human Blood. *Acs Nano* **2014**, *8*, 2667-2676.

(2) Eck, W.; Craig, G.; Sigdel, A.; Ritter, G.; Old, L. J.; Tang, L.; Brennan, M. F.; Allen, P. J.; Mason, M. D. PEGylated Gold Nanoparticles Conjugated to Monoclonal F19 Antibodies as Targeted Labeling Agents for Human Pancreatic Carcinoma Tissue. *ACS Nano* **2008**, *2*, 2263–2272.

(3) Grabarek, Z.; Gergely, J. Zero-Length Crosslinking Procedure with the use of Active Esters. *Anal. Biochem.* **1990**, *185*, 131–135.

(4) Kabashin, A. V.; Evans, P.; Pastkovsky, S.; Hendren, W.; Wurtz, G. A.; Atkinson, R.; Pollard, R.; Podolskiy, V. A.; Zayats, A. V. Plasmonic Nanorod Metamaterials for Biosensing. *Nat. Mater.* **2009**, *8*, 867-871.

(5) Voros, J. The Density and Refractive Index of Adsorbing Protein Layers. *Biophys. J.* **2004**, *87*, 553-561.

(6) Erickson, H. P. Size and Shape of Protein Molecules at the Nanometer Level Determined by Sedimentation, Gel Filtration, and Electron Microscopy. *Biol. Proced. Online.* **2009**, *15*, 32-51.

(7) De Boer, J. H. *The Dynamical Character of Adsorption, second ed.* (Oxford University Press, London, 1968).

(8) Nusz, G. J.; Curry, A. C.; Marinakos, S. M.; Wax, A.; Chilkoti, A. Rational Selection of Gold Nanorod Geometry for Lable-Free Plasmonic Biosensors. *ACS Nano* **2009**, *3*, 795-806.